
LEIBNIZ-INFORMATIONSZENTRUM
TECHNIK UND NATURWISSENSCHAFTEN
UNIVERSITÄTSBIBLIOTHEK



FAIR scientific information with the Open Research Knowledge Graph

Markus Stocker
December 13, 2022
e-IRG Workshop

failure than in LV tissue samples from unused donor hearts (Figure 1A). As shown by electrophoretic mobility shift assays, IRE binding activity was significantly reduced in failing hearts (most pronounced in patients with ischemic cardiomyopathy) (Figure 1B). Protein expression levels of the transferrin receptor were significantly lower in failing hearts than in the controls (Figure 1C).

Targeted *Irf* deletion in mice induces ID in the myocardium

We generated mice with a cardiomyocyte-targeted deletion of *Irf1* and *Irf2* (*Cre-Irf1/2^{fl}*) to address *Irf* function in the heart (Figure 2A). *Cre-Irf1/2^{fl}* mice were born at the expected Mendelian inheritance ratio and survived into adulthood. Reverse transcriptase polymerase chain reaction on LV myocardium and isolated cardiomyocytes demonstrated near-complete *Cre*-mediated deletion of *Irf1* and *Irf2* mRNAs in cardiomyocytes from *Cre-Irf1/2^{fl}* mice compared with littermates lacking the *Cre* transgene (*Irf1/2^{fl}*) (Figure 2B). *Irf1* and *Irf2* protein expression was markedly reduced in LV myocardium and barely detectable in isolated cardiomyocytes from *Cre-Irf1/2^{fl}* mice (Figure 2C and D). *Irf1* and *Irf2* protein expression in the liver was similar in *Cre-Irf1/2^{fl}* and *Irf1/2^{fl}* mice (Figure 2C and D). IRE binding activity was strongly reduced in isolated cardiomyocytes from *Cre-Irf1/2^{fl}* mice (Figure 2E), confirming near-complete *Cre*-mediated recombination. Iron-regulatory protein/IRE-regulated proteins involved in iron transport and storage were differentially

regulated in cardiomyocytes from *Cre-Irf1/2^{fl}* mice: the transferrin receptor was down-regulated ($25 \pm 14\%$ of *Irf1/2^{fl}* controls, $P=0.006$), whereas ferroportin ($325 \pm 9\%$, $P=0.003$) and ferritin H-chain ($249 \pm 35\%$, $P=0.012$) were up-regulated ($n=3$ per group; representative immunoblots are presented in Figure 2F). As a result, iron concentration in cardiomyocytes was significantly reduced in *Cre-Irf1/2^{fl}* mice (Figure 2G). Likewise, iron concentration in the left ventricle was reduced in *Cre-Irf1/2^{fl}* mice compared with *Irf1/2^{fl}* controls, whereas iron concentrations in the M. quadriceps femoris and liver were not affected (Figure 2H). Iron concentration in the left ventricle was normal in *Cre* mice showing that cardiac ID in *Cre-Irf1/2^{fl}* mice was not related to *Cre* transgene expression per se (Figure 2H). Haem and myoglobin concentrations were significantly reduced in the left ventricle of *Cre-Irf1/2^{fl}* mice (Figure 2I and J). Copper and free radical concentrations in the left ventricle were similar in *Cre-Irf1/2^{fl}* and *Irf1/2^{fl}* mice (see Supplementary material online, Figure S2).

Cre-Irf1/2^{fl} mice did not show an obvious phenotype under baseline conditions. Body mass, heart mass, LV mass, and cardiomyocyte cross-sectional area were similar in *Cre-Irf1/2^{fl}* and *Irf1/2^{fl}* mice under baseline conditions (see Supplementary material online, Table S1). On echocardiography, LV end-diastolic and end-systolic dimensions and LV systolic and diastolic function were similar in both genotypes (see Supplementary material online, Table S1). *Cre-Irf1/2^{fl}* mice were not anaemic and had a normal peripheral blood count (see Supplementary material online, Table S2).

Scientific information is data
This data is not FAIR
Certainly not for machines

We find and access documents

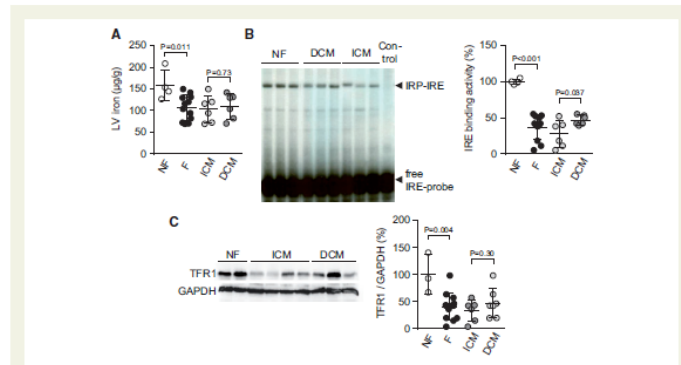


Figure 1 Reduced IRE activity and iron content in failing human hearts. (A) Non-haem iron concentration in left ventricular (LV) tissue samples from non-failing donors (NF) and patients with cardiac failure (F) due to ischemic cardiomyopathy (ICM) or dilated cardiomyopathy (DCM); $n=4-6$ per group. (B) Representative electrophoretic mobility shift assay and summary data showing iron-responsive element (IRE) binding activity in LV tissue samples; $n=4-6$ (control, no sample loaded). (C) Representative immunoblot and summary data showing transferrin receptor 1 (TFR1) and GAPDH protein expression in LV tissue samples; $n=3-7$. P-values were determined by two independent sample *t*-test.

failure than in LV tissue samples from unused donor hearts (Figure 1A). As shown by electrophoretic mobility shift assays, IRE binding activity was significantly reduced in failing hearts (most pronounced in patients with ischemic cardiomyopathy) (Figure 1B). Protein expression levels of the transferrin receptor were significantly lower in failing hearts than in the controls (Figure 1C).

Targeted *Irf* deletion in mice induces ID in the myocardium

We generated mice with a cardiomyocyte-targeted deletion of *Irf1* and *Irf2* (*Cre-Irf1/2^{fl}*) to address *Irf* function in the heart (Figure 2A). *Cre-Irf1/2^{fl}* mice were born at the expected Mendelian inheritance ratio and survived into adulthood. Reverse transcriptase polymerase chain reaction on LV myocardium and isolated cardiomyocytes demonstrated near-complete *Cre*-mediated deletion of *Irf1* and *Irf2* mRNAs in cardiomyocytes from *Cre-Irf1/2^{fl}* mice compared with littermates lacking the *Cre* transgene (*Irf1/2^{fl}*) (Figure 2B). *Irf1* and *Irf2* protein expression was markedly reduced in LV myocardium and barely detectable in isolated cardiomyocytes from *Cre-Irf1/2^{fl}* mice (Figure 2C and D). *Irf1* and *Irf2* protein expression in the liver was similar in *Cre-Irf1/2^{fl}* and *Irf1/2^{fl}* mice (Figure 2C and D). IRE binding activity was strongly reduced in isolated cardiomyocytes from *Cre-Irf1/2^{fl}* mice (Figure 2E), confirming near-complete *Cre*-mediated recombination. Iron-regulatory protein/IRE-regulated proteins involved in iron transport and storage were differentially

regulated in cardi-

per group, representative (Figure 2F). As a result, iron concentration in the left ventricle was significantly reduced in *Irf1/2^{fl}* mice compared with littermates in the M. quadriceps (Figure 2H). Iron concentration in the left ventricle of *Cre-Irf1/2^{fl}* mice showing that it related to *Cre* transgene and myoglobin concentration in the left ventricle of *Cre-Irf1/2^{fl}* mice (Figure 2I and J). Copper and free radical concentrations in the left ventricle were similar in *Cre-Irf1/2^{fl}* and *Irf1/2^{fl}* mice (see Supplementary material online, Figure S2).

Cre-Irf1/2^{fl} mice did not show an obvious phenotype under baseline conditions. Body mass, heart mass, LV mass, and cardiomyocyte cross-sectional area were similar in *Cre-Irf1/2^{fl}* and *Irf1/2^{fl}* mice under baseline conditions (see Supplementary material online, Table S1). On echocardiography, LV end-diastolic and end-systolic dimensions and LV systolic and diastolic function were similar in both genotypes (see Supplementary material online, Table S1). *Cre-Irf1/2^{fl}* mice were not anemic and had a normal peripheral blood count (see Supplementary material online, Table S2).

failure than in LV tissue samples from unused donor hearts (Figure 1A). As shown by electrophoretic mobility shift assays, IRE binding activity was significantly reduced in failing hearts (most pronounced in patients with ischemic cardiomyopathy) (Figure 1B). Protein expression levels of the transferrin receptor were significantly lower in failing hearts than in the controls (Figure 1C).

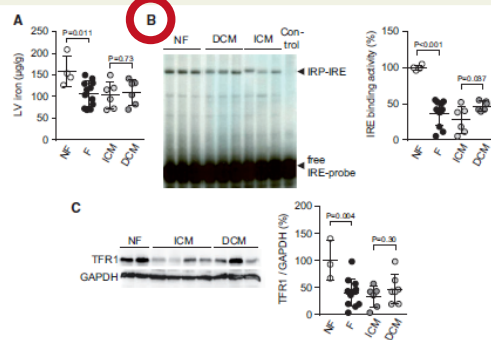


Figure 1 Reduced IRE activity and iron content in failing human hearts. (A) Non-haem iron concentration in left ventricular (LV) tissue samples from non-failing donors (NF) and patients with cardiac failure (F) due to ischemic cardiomyopathy (ICM) or dilated cardiomyopathy (DCM); $n=4-6$ per group. (B) Representative electrophoretic mobility shift assay and summary data showing iron-responsive element (IRE) binding activity in LV tissue samples; $n=4-6$ (control; no sample loaded). (C) Representative immunoblot and summary data showing transferrin receptor 1 (TFR1) and GAPDH protein expression in LV tissue samples; $n=3-7$. P-values were determined by two independent sample t-test.

failure than in LV tissue samples from unused donor hearts (Figure 1A). As shown by electrophoretic mobility shift assays, IRE binding activity was significantly reduced in failing hearts (most pronounced in patients with ischemic cardiomyopathy) (Figure 1B). Protein expression levels of the transferrin receptor were significantly lower in failing hearts than in the controls (Figure 1C).

Targeted *Irf* deletion in mice induces ID in the myocardium

We generated mice with a cardiomyocyte-targeted deletion of *Irf1* and *Irf2* (*Cre-Irf1/2^{fl/fl}*) to address *Irf* function in the heart (Figure 2A). *Cre-Irf1/2^{fl/fl}* mice were born at the expected Mendelian inheritance ratio and survived into adulthood. Reverse transcriptase polymerase chain reaction on LV myocardium and isolated cardiomyocytes demonstrated near-complete *Cre*-mediated deletion of *Irf1* and *Irf2* mRNAs in cardiomyocytes from *Cre-Irf1/2^{fl/fl}* mice compared with littermates lacking the *Cre* transgene (*Irf1/2^{fl/fl}*) (Figure 2B). *Irf1* and *Irf2* protein expression was markedly reduced in LV myocardium and barely detectable in isolated cardiomyocytes from *Cre-Irf1/2^{fl/fl}* mice (Figure 2C and D). *Irf1* and *Irf2* protein expression in the liver was similar in *Cre-Irf1/2^{fl/fl}* and *Irf1/2^{fl/fl}* mice (Figure 2C and D). IRE binding activity was strongly reduced in isolated cardiomyocytes from *Cre-Irf1/2^{fl/fl}* mice (Figure 2E), confirming near-complete *Cre*-mediated recombination. Iron-regulatory protein/IRE-regulated proteins involved in iron transport and storage were differentially

regulated in cardi-

per group, representative (Figure 2F). As a result, iron content was significantly reduced in *Cre-Irf1/2^{fl/fl}* mice compared with *Irf1/2^{fl/fl}* mice (Figure 2H). Iron concentration in the left ventricle of *Cre-Irf1/2^{fl/fl}* mice was similar to *Irf1/2^{fl/fl}* mice (see Supplementary material online, Figure S2).

Cre-Irf1/2^{fl/fl} mice did not show an obvious phenotype under baseline conditions. Body mass, heart mass, LV mass, and cardiomyocyte cross-sectional area were similar in *Cre-Irf1/2^{fl/fl}* and *Irf1/2^{fl/fl}* mice under baseline conditions (see Supplementary material online, Table S1). On echocardiography, LV end-diastolic and end-systolic dimensions and LV systolic and diastolic function were similar in both genotypes (see Supplementary material online, Table S1). *Cre-Irf1/2^{fl/fl}* mice were not anemic and had a normal peripheral blood count (see Supplementary material online, Table S2).

failure than in LV tissue samples from unused donor hearts (Figure 1A). As shown by electrophoretic mobility shift assays, IRE binding activity was significantly reduced in failing hearts (most pronounced in patients with ischemic cardiomyopathy) (Figure 1B). Protein expression levels of the transferrin receptor were significantly lower in failing hearts than in the controls (Figure 1C).

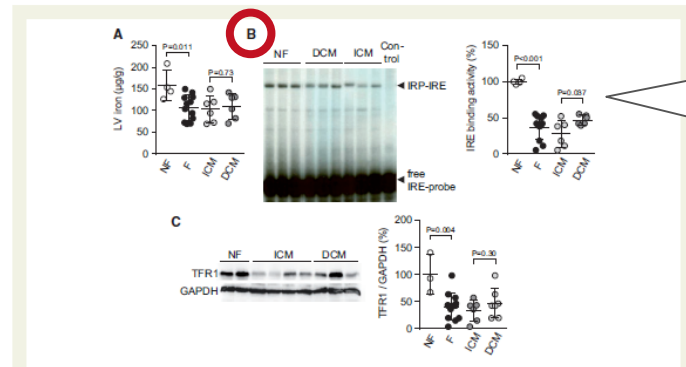
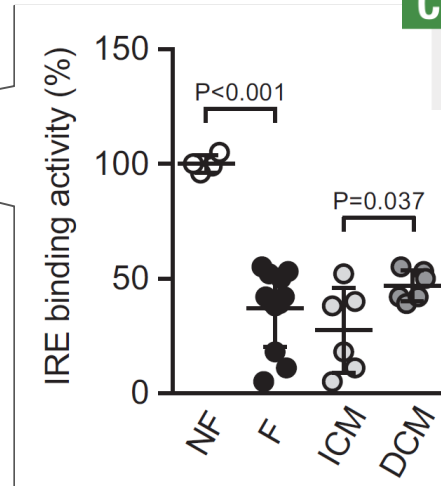


Figure 1 Reduced IRE activity and iron content in failing human hearts. (A) Non-haem iron concentration in left ventricular (LV) tissue samples from non-failing donors (NF) and patients with cardiac failure (F) due to ischemic cardiomyopathy (ICM) or dilated cardiomyopathy (DCM); $n = 4-6$ per group. (B) Representative electrophoretic mobility shift assay and summary data showing iron-responsive element (IRE) binding activity in LV tissue samples; $n = 4-6$ (control; no sample loaded). (C) Representative immunoblot and summary data showing transferrin receptor 1 (TFR1) and GAPDH protein expression in LV tissue samples; $n = 3-7$. P values were determined by two independent sample *t*-test.



CSV

failure than in LV tissue samples from unused donor hearts (Figure 1A). As shown by electrophoretic mobility shift assays, IRE binding activity was significantly reduced in failing hearts (most pronounced in patients with ischemic cardiomyopathy) (Figure 1B). Protein expression levels of the transferrin receptor were significantly lower in failing hearts than in the controls (Figure 1C).

Targeted *Irf* deletion in mice induces ID in the myocardium

We generated mice with a cardiomyocyte-targeted deletion of *Irf1* and *Irf2* (*Cre-Irf1/2^{fl}*) to address *Irf* function in the heart (Figure 2A). *Cre-Irf1/2^{fl}* mice were born at the expected Mendelian inheritance ratio and survived into adulthood. Reverse transcriptase polymerase chain reaction on LV myocardium and isolated cardiomyocytes demonstrated near-complete *Cre*-mediated deletion of *Irf1* and *Irf2* mRNAs in cardiomyocytes from *Cre-Irf1/2^{fl}* mice compared with littermates lacking the *Cre* transgene (*Irf1/2^{fl}*) (Figure 2B). *Irf1* and *Irf2* protein expression was markedly reduced in LV myocardium and barely detectable in isolated cardiomyocytes from *Cre-Irf1/2^{fl}* mice (Figure 2C and D). *Irf1* and *Irf2* protein expression in the liver was similar in *Cre-Irf1/2^{fl}* and *Irf1/2^{fl}* mice (Figure 2C and D). IRE binding activity was strongly reduced in isolated cardiomyocytes from *Cre-Irf1/2^{fl}* mice (Figure 2E), confirming near-complete *Cre*-mediated recombination. Iron-regulatory protein/IRE-regulated proteins involved in iron transport and storage were differentially

regulated in cardi-

per group, representative (Figure 2F). As a result, iron content was significantly reduced in *Cre-Irf1/2^{fl}* mice compared with *Irf1/2^{fl}* mice (Figure 2H). Iron concentration in the left ventricle of *Cre-Irf1/2^{fl}* mice was similar to *Irf1/2^{fl}* mice (see Supplementary material online, Figure S2).

Cre-Irf1/2^{fl} mice did not show an obvious phenotype under baseline conditions. Body mass, heart mass, LV mass, and cardiomyocyte cross-sectional area were similar in *Cre-Irf1/2^{fl}* and *Irf1/2^{fl}* mice under baseline conditions (see Supplementary material online, Table S1). On echocardiography, LV end-diastolic and end-systolic dimensions and LV systolic and diastolic function were similar in both genotypes (see Supplementary material online, Table S1). *Cre-Irf1/2^{fl}* mice were not anemic and had a normal peripheral blood count (see Supplementary material online, Table S2).

failure than in LV tissue samples from unused donor hearts (Figure 1A). As shown by electrophoretic mobility shift assays, IRE binding activity was significantly reduced in failing hearts (most pronounced in patients with ischemic cardiomyopathy) (Figure 1B). Protein expression levels of the transferrin receptor were significantly lower in failing hearts than in the controls (Figure 1C).

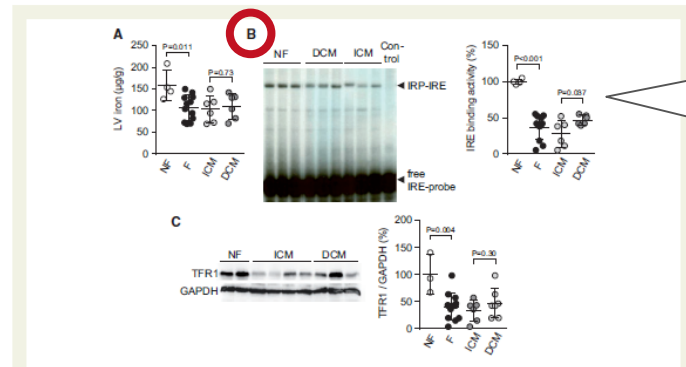
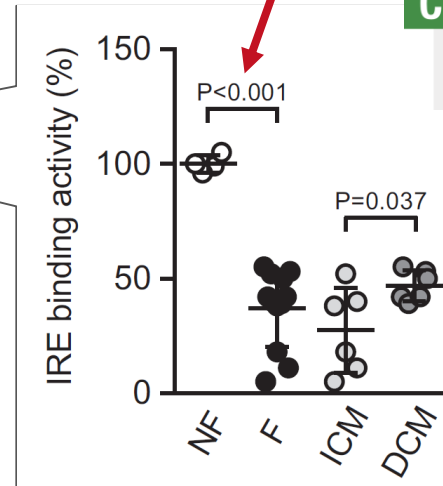


Figure 1 Reduced IRE activity and iron content in failing human hearts. (A) Non-haem iron concentration in left ventricular (LV) tissue samples from non-failing donors (NF) and patients with cardiac failure (F) due to ischemic cardiomyopathy (ICM) or dilated cardiomyopathy (DCM); $n = 4-6$ per group. (B) Representative electrophoretic mobility shift assay and summary data showing iron-responsive element (IRE) binding activity in LV tissue samples; $n = 4-6$ (control, no sample loaded). (C) Representative immunoblot and summary data showing transferrin receptor 1 (TFR1) and GAPDH protein expression in LV tissue samples; $n = 3-7$. P values were determined by two independent sample *t*-test.



CSV

This is what machines should consume

Targeted Irf deletion in mice induces ID in the myocardium

We generated mice with a cardiomyocyte-targeted deletion of

Iron concentration in the left ventricle (LV) of mice compared with Irf1^{+/+} mice (Figure 2H). Iron concentration

patients with ischemic cardiomyopathy) (Figure 1B). Protein expression levels of the transferrin receptor were significantly lower in fail-

Student's t-test [http://purl.obolibrary.org/obo/OBI_0000739]

has dependent variable

iron-responsive element binding [<http://amigo.geneontology.org/amigo/term/GO:0030350>]

has specified input

<https://doi.org/10.4563/zenodo.56980>

CSV

has specified output

p-value [http://purl.obolibrary.org/obo/OBI_0000175]

scalar value specification "0.0000000131112475"^^xsd:decimal

Figure 1 Reduced IRP activity and iron content in failing human hearts. (A) Non-haem iron concentration in left ventricular (LV) tissue samples from non-failing donors (NF) and patients with cardiac failure (F) due to ischemic cardiomyopathy (ICM) or dilated cardiomyopathy (DCM); n=4-6 per group. (B) Representative electrophoretic mobility shift assay and summary data showing iron-responsive element (IRE) binding activity in LV tissue samples; n=4-6 (control, no sample loaded). (C) Representative immunoblot and summary data showing transferrin receptor 1 (TFR1) and GAPDH protein expression in LV tissue samples; n=3-7. P-values were determined by two independent sample t-test.

“Scientific writing can [...] be called *information burying*”

First we bury it and then we mine it again

-- Barend Mons (2005)

<https://doi.org/10.1186/1471-2105-6-142>

“we have failed to [...] organize [...] information [...] in rigorous [...] ways,
so that finding what we want and understanding what's already known
become [...] increasingly costly experiences”

-- Teresa K. Attwood et al. (2009)

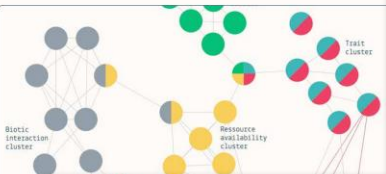
<https://doi.org/10.1042/BJ20091474>

“Despite recent developments in machine learning [...],
data extraction is still largely a manual process”

-- Julian Higgins et al. (2022)

<https://training.cochrane.org/handbook/current>

Interactive visualisation
understanding of s



Search

Browse State-of-the-Art Datasets Methods

Top Social New Greatest

Trending Research



TAP-Vid: A Benchmark for Tracking Any Point in Time

deepmind/tapnet • TensorFlow • 7 Nov 2022

Generic motion understanding from video involves not only tracking their surfaces deform and move.

Optical Flow Estimation



Real-Time Target Sound Extraction

vb000/waveformer • Pytorch • 4 Nov 2022

We present the first neural network model to achieve real-time a

Cooperation Databank

- Data overview
- Meta-analysis
- Meta-regression
- Citation explorer
- Ontology explorer
- Add Study
- Tutorials
- Website

Feedback?

Please let us know

Overview of the studies

1809

Number of papers

2636

Number of studies

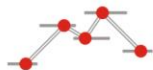
13934

Number of effects

Show studies by
Country/Region Year of data collection Sample size



MetaLab Explore Data Documentation Publications Team



MetaLab

Interactive, community-augmented meta-analysis
tools for cognitive development research

New: The 2020 Contribution Challenge Winners

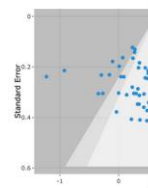
Explore Apps

View Documentation

New MetaLab User? Check out Getting Started first!

The MetaLab database contains 2,497 effect
sizes from 30 meta-analyses
of cognitive development
papers and 45,260 subjects

Funnel plot of bias in effect sizes



Domains



Early Language

How do children learn their native language?



Cognitive Development

What is the nature of children's cognitive development?

COVID-19 Air Quality Data Collection

Home Search database Download data Submit data Contact Links

COVID-19 Air Quality Data Collection

Publications per Country/Region that address the impacts of COVID-19 lockdowns on air quality:



TREATMENTBANK BIODIVERSITY LITERATURE REPOSITORY SERVICES HOW TO PARTICIPATE ABOUT



Arcadia Fund supports Plazi in its endeavor to rediscover known biodiversity

Plazi will utilize a grant from Arcadia Fund to accelerate discovery of known biodiversity by expanding the existing corpus of the Biodiversity Literature Repository [more](#)

Access to taxonomic treatments mentioned in press releases

Result of an experiment to test how easy it is to locate the original taxonomic treatments of species mentioned in press releases [more](#)

New Species of 2021

Here we present a small selection of 12 spectacular species that were newly discovered in 2021 with links to their complete taxonomic treatment. [more](#)

Annotating genes sequences with data from herbarium sheets and publications

A report on a workshop on updating accession with specimen-data from publications [more](#)

STATS

Articles: 56539
Treatments: 808577
Occurrences: 265911
Material Citations (MC): 1267991
Geo-referenced MC: 375379

EVENTS

TAGS

ABOUT (8) BICHL (1) BLR (1)
BLUE LIST (1) DAK (1)
DATA API AND TOOLS (13) DATA QUALITY (1)
EVENTS (18) GOLDEN GATE (2) LECTURES (1)
LEGAL ISSUES (8) MEMBERS (1) NEWS (20)
PARTNERS (1) PROJECTS (1)
PUBLICATIONS (1) REPOS (1) SERVICES (1)
SOURCE CODE (1) TREATMENT BANK (10)

SOCIAL

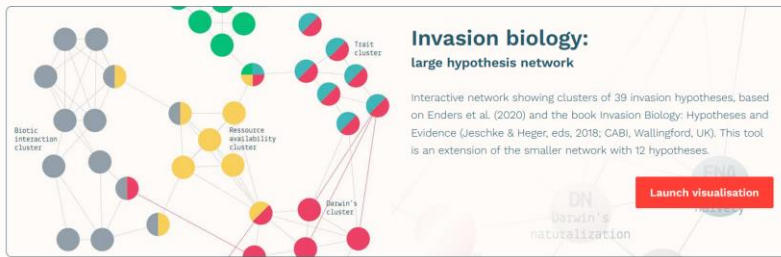
Twitter

GitHub

info@plazi.org

Vimeo

Interactive visualisation tools for a better understanding of science and nature



Trending Research



TAP-Vid: A Benchmark for Tracking Any Point in a Video

by deepmind/ageron • 7 Nov 2022

Generic motion understanding from video involves not only tracking objects, but also perceiving how their surfaces deform and move.

Optical Flow Estimation



Real-Time Target Sound Extraction

by v6000/waveburner • 4 Nov 2022

We present the first neural network model to achieve real-time and streaming target sound extraction.

Tools for cognitive development research

New: The 2020 Contribution Challenge Winners

Let Explore Apps View Documentation

New Metalab User? Check out Getting Started

5.0 stars / hour

Play

Code

Domains

★ 86

5.0 stars / hour

Early Language

How do children learn their native language?

Code

COVID-19 Air Quality Data Collection

Publishes daily/region that address the impacts of COVID-19 lockdowns on air quality.

13934

Number of cities

356283

Total participants

Show results by
Country/region Year of data collection Sample size

Number of queries (top world per country)

Participation map

Participation map

Participation map

Participation map

Participation map

Participation map

Participation map

Participation map

Participation map

Participation map

Participation map

Participation map

Participation map

Participation map

Participation map

Participation map

Participation map

Participation map

Participation map

Participation map

Participation map

Participation map

Participation map

Participation map

Participation map

Participation map

Participation map

Participation map

Participation map

Participation map

Participation map

Participation map

Participation map

Participation map

Participation map

Participation map

Participation map

Participation map

Participation map

Participation map

Participation map

Participation map

Participation map

Participation map

Participation map

Participation map

Participation map

Participation map

Participation map

Participation map

Participation map



Arcadia Fund supports Plazi in its endeavor to rediscover known biodiversity

May 16, 2022

Plazi will utilize a grant from Arcadia Fund to accelerate discovery of known biodiversity by expanding the existing corpus of the Biodiversity Literature Repository [more](#)

Access to taxonomic treatments mentioned in press releases

Jan 14, 2022

Result of an experiment to test how easy it is to locate the original taxonomic treatments of species mentioned in press releases [more](#)

New Species of 2021

Dec 22, 2021

Here we present a small selection of 12 spectacular species that were newly discovered in 2021 with links to their complete taxonomic treatment. [more](#)

Annotating genes sequences with data from herbarium sheets and publications

Nov 11, 2021

A report on a workshop on updating accession with specimen-data from publications [more](#)

STATS

Articles: 56539
Treatments: 808577
Occurrences: 265911
Material Citations (MC): 1267991
Geo-referenced MC: 375379

EVENTS

TAGS

ABOUT (8) BICHL (1) BLR (1)
BLUE LIST (1) DAK (1)
DATA, API AND TOOLS (13) DATA QUALITY (1)
EVENTS (18) GOLDEN GATE (2) LECTURES (1)
LEGAL ISSUES (8) MEMBERS (1) NEWS (20)
PARTNERS (1) PROJECTS (1)
PUBLICATIONS (1) REPOS (1) SERVICES (1)
SOURCE CODE (1) TREATMENT BANK (10)

SOCIAL

Twitter

GitHub

info@plazi.org

Vimeo

Cooperation DataBank

Overview of the studies

1809	2636	13934	356283
Number of papers	Number of studies	Number of effects	Total participants

Show studies by

☒ Country/Region ☐ Year of data collection ☐ Sample size

Number of studies (log-scale) per country

Feedback?

Please let us know.

Select studies

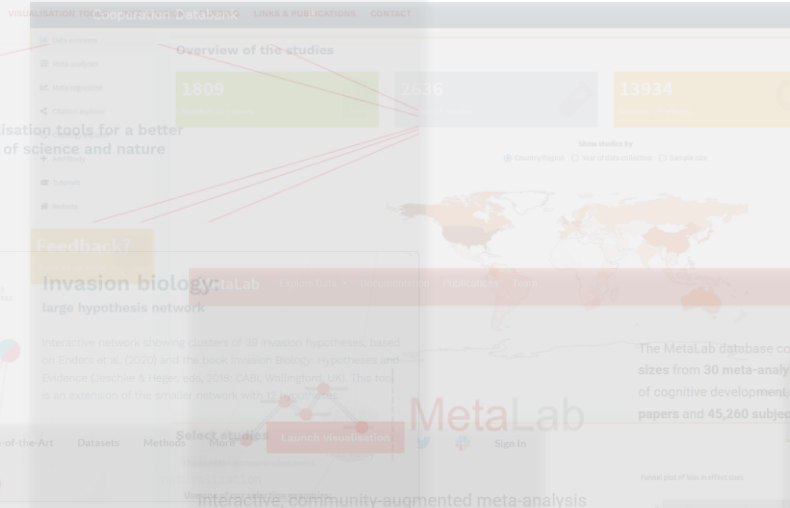
Choose inclusion criteria to select studies.

Use one of our selection examples:

*Please allow some time for the data to update.

Select...

Interactive visualisation tools for a better understanding of science and nature



Trending Research

TAP-Vid: A Benchmark for Tracking Any Point in Video

↳ deepmind/lapnet • 🌟 7 Nov 2022

Generic motion understanding from video involves not only tracking objects, but also perceiving how their surfaces deform and move.

Optical Flow Estimation

Real-Time Target Sound Extraction

↳ v6000/waveformer • 🌟 4 Nov 2022

We present the first neural network model to achieve real-time and streaming target sound extraction.

Early Language

How do children learn their native language?

Domains

Cognitive Development

What is the nature of children's cognitive development?

Access to taxonomic treatments mentioned in press releases

Result of an experiment to test how easy it is to locate the original taxonomic treatments of species mentioned in press releases more

New Species of 2021

Here we present a small selection of 12 spectacular species that were newly discovered in 2021 with links to their complete taxonomic treatment. more



Aquatic Biodiversity

May 16, 2022

Aquatic Biodiversity supports its endeavor to rediscover known biodiversity

Access to taxonomic treatments mentioned in press releases

Jan 14, 2022

Result of an experiment to test how easy it is to locate the original taxonomic treatments of species mentioned in press releases more

New Species of 2021

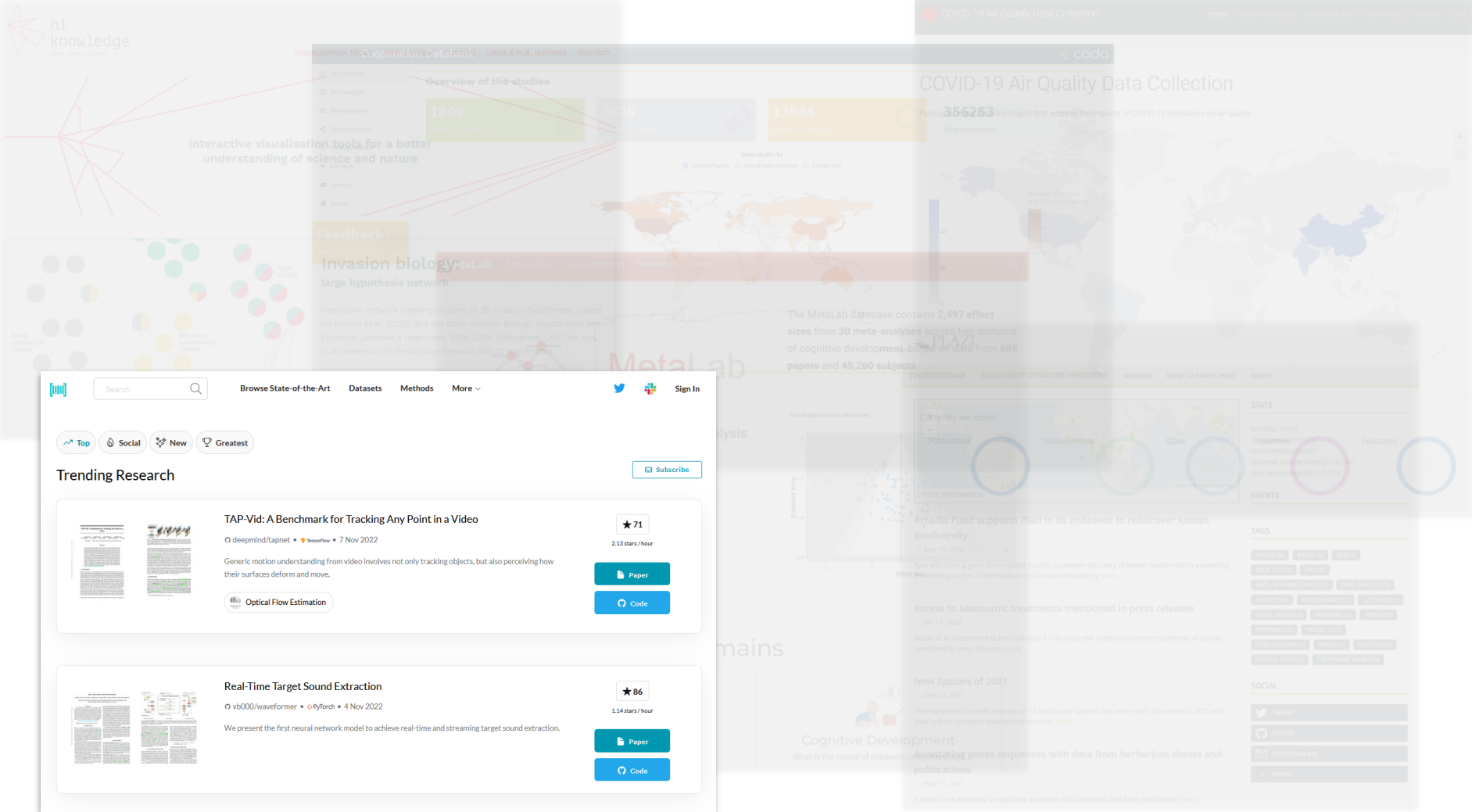
Dec 22, 2021

Here we present a small selection of 12 spectacular species that were newly discovered in 2021 with links to their complete taxonomic treatment. more

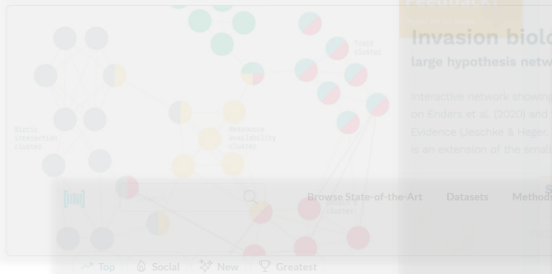
Accessing genes sequences with data from herbarium sheets and publications

Nov 11, 2021

A report on a workshop on updating accessions with specimen data from publications more



Interactive visualisation tools for a better understanding of science and nature



Trending Research



TAP-Vid: A Benchmark for Tracking Any Point

by deepmind/ageron • 7 Nov 2022

Generative motion understanding from video involves not only tracking their surfaces deforms and move.

Optical Flow Estimation



Real-Time Target Sound Extraction

by v6000/waveformer • 4 Nov 2022

We present the first neural network model to achieve real-time

Overview of the studies

1809
Number of studies

2436
Number of studies

13934
Number of studies

355283
Total participants

Show studies by

Country/region Year of data collection Sample size



COVID-19 Air Quality Data Collection

Publicly available data from many regions that address the impacts of COVID-19 lockdowns on air quality.



MetaLab

Explore Data • Documentation Publications Team

The MetaLab database contains **2,497 effect sizes** from **30 meta-analyses** across two domains of cognitive development, based on data from **688 papers** and **45,260 subjects**.

Interactive, community-augmented meta-analysis tools for cognitive development research

New: The 2020 Contribution Challenge Winners

[Explore Apps](#) [View Documentation](#)

New MetaLab User? Check out [Getting Started](#) first!

Domains

Early Language

How do children learn their native language?

Cognitive Development

What is the nature of children's understanding?

Scholarly Knowledge. FAIR.

The Open Research Knowledge Graph (ORKG) aims to describe research papers in a structured manner. With the ORKG, papers are easier to find and compare. [Play video](#)

Browse by research field

Search for fields...

Arts and Humanities
91 papers

Engineering
1786 papers

Life Sciences
4238 papers

Physical Sciences &
Mathematics
3309 papers

Social and Behavioral Sciences
716 papers

Comparisons

Visual

Code-switched corpora for Named Entity Recognition (NER)

7 Contributions 0 Visualizations 07-09-2022

This comparison takes a comprehensive look at various corpora in language context for the NLP/IE Named Entity Recognition (NER) over all t...

A Comparison of Scientific Publications on the State-of-the-art in Requirements Engineering and Software Engineering

5 Contributions 0 Visualizations 11-09-2022

This comparison provides an overview of scientific publications that have investigated primary studies in requirements engineering and software engineering to give a snapshot of the "current" state...

Versions: Version 09-09-2022 • View history

Named Entity Recognition in the Computational Natural Language Learning (CoNLL) Series

2 Contributions 0 Visualizations 15-08-2022

The NER shared tasks organized in the Conference on Computational Natural Language Learning

Natural Language ...

Open Research Knowledge Graph

<https://orkg.org> • [@orkg_org](#)

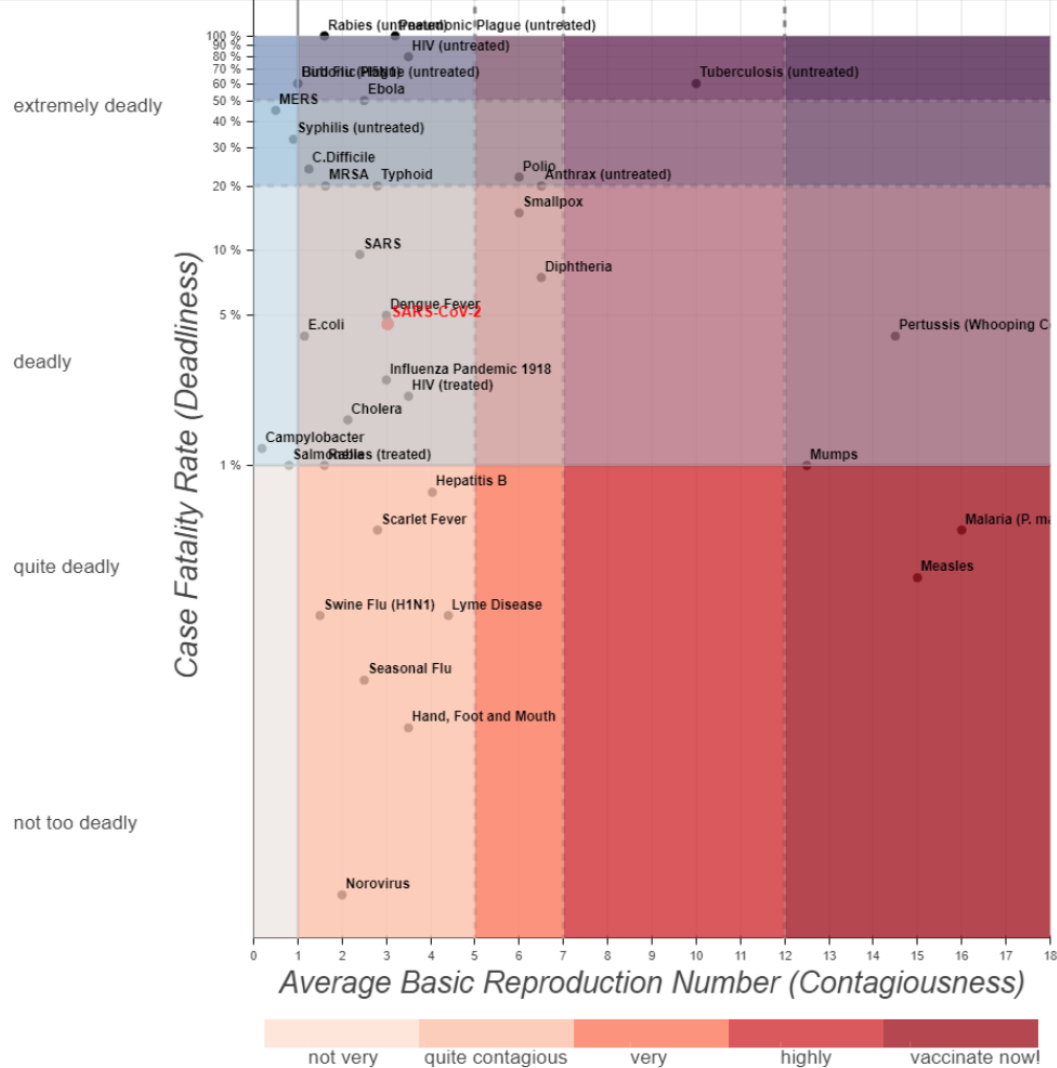
Observatories

[More observatories](#)

Artificial Intelligence

This observatory will comprise descriptions and comparisons of research approaches in the context ...

Properties	The early phase of the COVID-19 outbreak in Lombardy, Italy 2020 - Contribution 1	Transmission potential of COVID-19 in Iran 2020 - Contribution 1	Transmission potential of COVID-19 in Iran 2020 - Contribution 2	Estimating the generation interval for COVID-19 based on symptom onset data 2020 - Contribution 1
location	Lombardy, Italy	Iran	Iran	Singapore
Time period	Time interval	Time interval	Time interval	Time interval
has beginning	2020-01-14	2020-02-19	2020-02-19	2020-01-21
has end	2020-03-08	2020-02-29	2020-02-29	2020-02-26
Basic reproduction number	Basic reproduction number estimate value specification	Basic reproduction number estimate value specification	Basic reproduction number estimate value specification	Basic reproduction number estimate value specification
Has value	3.1	3.6	3.58	1.27
Confidence interval (95%)	Confidence interval (95%)	Confidence interval (95%)	Confidence interval (95%)	Confidence interval (95%)
Lower confidence limit	2.9	3.4	1.29	1.19
Upper confidence limit	3.2	4.2	8.46	1.36



Transmission potential of COVID-19 in Iran 2020 - Contribution 2		Estimating the generation interval for COVID-19 based on symptom onset data 2020 - Contribution 1	
ResetTool, SaveTool, PanTool, DatetimeTickFormatter, Whisker			
org/orkg/simcomp')		Iran	
s_end', :]])		Singapore	
Time interval		Time interval	
ver confidence limit', :]])		2020-01-21	
per confidence limit', :]])		2020-02-19	
2020-02-29		2020-02-26	
Basic reproduction number estimate value specification		Basic reproduction number estimate value specification	
3.58		1.27	
Confidence interval (95%)		Confidence interval (95%)	
1.29		1.19	
oper=upper))		1.36	
8.46			
lot_height=350, tools=[hover1, WheelZoomTool(), PanTool(), ResetTool(),			

```
[ ]: import requests
import datetime
import pandas as pd
import numpy as np
from orkg import ORKG
from bokeh.io import export_png
from bokeh.models import ColumnDataSource, HoverTool, WheelZoomTool, ResetTool, SaveTool, PanTool, DatetimeTickFormatter, Whisker
from bokeh.plotting import figure, show, output_notebook

output_notebook()
```

```
[ ]: orkg = ORKG(host='https://orkg.org/orkg', simcomp_host='https://orkg.org/orkg/simcomp')

df = orkg.contributions.compare_dataframe(comparison_id='R44930')
```

```
[ ]: dates = np.array([datetime.date.fromisoformat(x) for x in df.loc['has end', :]])
values = np.float32(df.loc['Has value', :])
lower = np.array([np.float32(x) if x else np.nan for x in df.loc['Lower confidence limit', :]])
upper = np.array([np.float32(x) if x else np.nan for x in df.loc['Upper confidence limit', :]])
```

```
[ ]: hover1 = HoverTool(
    tooltips=[
        ('Date', '@date{%F}'),
        ('R0', '@value{0.ff}'),
        ('95% CI', '@lower{0.ff}~@upper{0.ff}')
    ],
    formatters={
        '@date': 'datetime',
        '@{value}': 'printf',
        '@{lower}': 'printf',
        '@{upper}': 'printf'
    }
)
```

```
df = pd.DataFrame(data=dict(date=dates, value=values, lower=lower, upper=upper))
source = ColumnDataSource(df)
p = figure(x_axis_type="datetime", y_range=(0, 9), plot_width=800, plot_height=350, tools=[hover1, WheelZoomTool(), PanTool(), ResetTool()],
p.xaxis.formatter=DatetimeTickFormatter(days=['%d %b']))
```

1 Work

Publication Year

☐ 2020

1

Work Type

☐ Dataset

1

License

☐ CC-BY-SA-4.0

1

COVID-19 Reproductive Number Estimates

Allard Oelen, Jennifer D'Souza, Markus Stocker, Lars Vogt, Kheir Eddine Farfar, Muhammad Haris, Kamel Fadel, Mohamad Yaser Jaradeh & Vitalis Wiens

Comparison published 2020 in [Open Research Knowledge Graph \(ORKG\)](#)

Comparison of published reproductive number estimates for the COVID-19 infectious disease

DOI registered October 16, 2020 via DataCite.



Dataset

English

 <https://doi.org/10.48366/r44930>



<https://doi.org/10.1101/2020.03.08.20030643>

Transmission potential of COVID-19 in Iran

Kamalich Muniz-Rodriguez, Isaac Chun-Hai Fung, Shayesterh R. Ferdosi, Sylvia K. Ofori, Yiseul Lee, Amna Tariq & Gerardo Chowell

Posted Content published 2020 via medRxiv

We computed reproduction number of COVID-19 epidemic in Iran using two different methods. We estimated R_0 at 3.6 (95% CI, 3.2, 4.2) (generalized growth model) and at 3.58 (95% CI, 1.29, 8.46) (estimated epidemic doubling time of 1.20 (95% CI, 1.05, 1.44) days) respectively. Immediate social distancing measures are recommended.

Other Identifiers

Publisher ID: [medrxiv;2020.03.08.20030643v1](https://doi.org/10.1101/2020.03.08.20030643v1)

DOI registered April 10, 2020 via Crossref.

2 Citations

Posted Content

<https://doi.org/10.1101/2020.03.08.20030643>



2 Citations

COVID-19 Reproductive Number Estimates

Allard Oelen, Jennifer D'Souza, Markus Stocker, Lars Vogt, Kheir Eddine Farfar, Muhammad Haris, Kamel Fadel, Mohamad Yaser

Jaradeh & Vitalis Wiens

Comparison published 2020 in [Open Research Knowledge Graph \(ORKG\)](#)

Comparison of published reproductive number estimates for the COVID-19 infectious disease

DOI registered October 16, 2020 via DataCite.



Dataset

English

<https://doi.org/10.48366/r44930>



Filter Works

Type to search...



Publication Year

☐ 2020

2

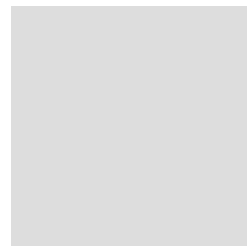
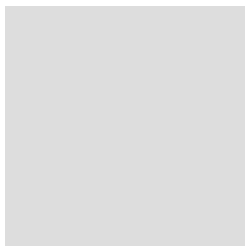
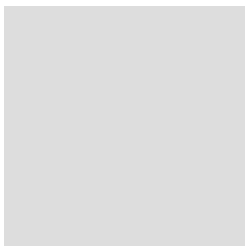
Work Type

☐ Dataset

1

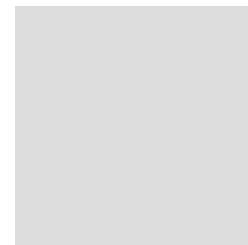
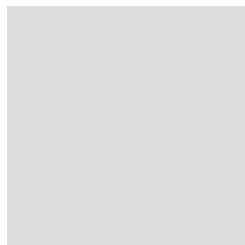
So why is most scientific information still buried in documents?

Because it is hard to produce FAIR scientific information



Basic reproduction number	<u>3.1</u>
	
location	<u>Lombardy, Italy</u>
	
Time period	<u>2020-01-14 - 2020-03-08</u>
	
research problem	<div> Determination of the COVID-19 <div>  </div> </div> <div> Cancel Create </div>
	<div> Determination of the COVID-19 basic reproduction number <div>  ORKG </div> </div> <div> → Referred: 35 times Instance of: Problem </div>

 Add property



The suggestions listed below are automatically generated based on the title and abstract from the paper. Using these suggestions is optional.

tract

+ Suggestions ?

References

Statements

Research problem

- « environmental phenomena
- « monitoring of atmospheric phenomena
- « organization and interpretation of sensor data
- « scientific computing workflows

Resource

- « Sensor Data

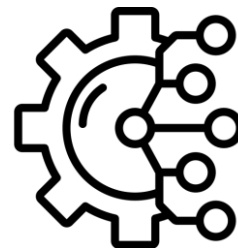


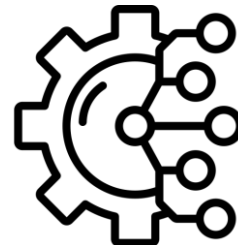
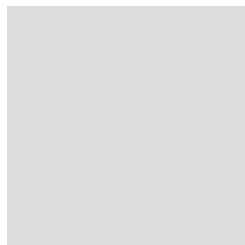
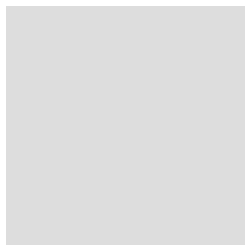
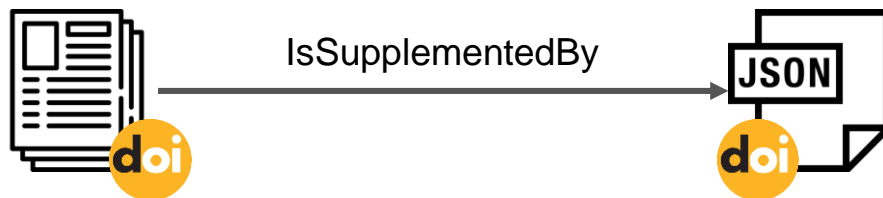
Production

```

32 # Two Linear Mixed Model (LMM) computations
33 lm.mwd.1 <- lmer(MWD_cor ~ cc_variant + (1|depth), data = df.MWD)
34 lm.mwd.2 <- lmer(MWD_cor ~ cc_type + (1|depth), data = df.MWD)
35
36 # Output data for the two LMM
37 df1 <- data.frame(summary(lm.mwd.1)$coefficients, check.names=FALSE)
38 df2 <- data.frame(summary(lm.mwd.2)$coefficients, check.names=FALSE)
39
40 instance <- tp$model_fitting(
41   label="Linear mixed model fitting with MWD as response, CC variant as predictor variable, and soil depth as random variable",
42   has_input_dataset=tuple(df.MWD, "Difference of mean weight diameter between the dry and wet sieving method"),
43   has_input_model=tp$statistical_model(
44     label="A linear mixed model with MWD as response and CC variant as predictor variable",
45     is_denoted_by=tp$formula(
46       label="The formula of the linear mixed model with MWD as response and CC variant as predictor variable",
47       has_value_specification=tp$value_specification(
48         label="MWD_cor ~ cc_variant + (1|depth)",
49         has_specified_value="MWD_cor ~ cc_variant + (1|depth)"
50       )
51     )
52   ),
53   has_output_dataset=tuple(df1, "Results of LMM with MWD as response and CC variant as predictor variable")
54 )
55 instance$serialize_to_file("article.contribution.1.json", format="json-ld")

```





Cover crops improve soil structure and change OC distribution in aggregate fractions ☆🔍

Soil Science

Gentsch, Norman

Laura Riechers, Florin

Boy, Jens

Schweneker, Dörte

Feuerstein, Ulf

Heuermann, Diana

Guggenberger, Georg

Published in: *SOIL*

Linear mixed model fitting with MWD a...

Linear mixed model fitting with MWD a...

has input dataset

<https://doi.org/10.5281/zenodo.7314152> ↗

has input model

[A linear mixed model with MWD as response > predictor variable](#)

has output dataset

[Results of LMM with MWD as response and CC var variable](#)

View Tabular Data: Results of LMM with MWD as response and CC variant as predictor variable

Pr(>|t|)

Search 7 records...

t value

Search 7 records...

df

Search 7 records...

8.689498e-05

14.46535

4.267258

0.04331638

2.069312

54.0

0.03388362

2.17684

54.0

0.08675521

1.744536

54.0

0.04539721

2.04838

54.0

0.03369833

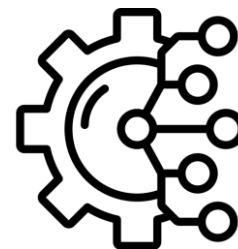
2.179203

54.0

0.001928021

3.260628

54.0



FAIR scientific information. It's time.